RESEARCH ON THE MUZZLE BLAST FLOW WITH GAS-PARTICLE MIXTURES BASED ON EULERIAN-EULERIAN APPROACH

C.-F. Zhuo W.-J. Yao* X.-S. Wu F. Feng
School of Mechanical Engineering
Nanjing University of Science and Technology
Nanjing, PR China

P. Xu
The Technical Center of Jinxi Industries Group Co.,Ltd
Taiyuan, PR China

ABSTRACT

The issue on the muzzle blast flow with gas-particle mixtures was numerically investigated in this paper. The propellant gas in the cannon was assumed to be gas-particle mixtures consisting of a variety of gaseous species and particles. The model made use of the Eulerian-Eulerican approach, where the particle were modeled as a second fluid with parameters like bulk density, velocity and temperature, interacting with the gas flow. A high-resolution upwind scheme(AUSMPW+) and detailed reaction kinetics model were employed to solve the chemical non-equilibrium Euler equations for gas phase. The Euler equations for particle phase were solved by MacCormack scheme. The particle diameter and the mass fraction of particle were tested to show their effects on the development process of muzzle blast flow with gas-particle mixtures. The distribution of the main flow parameters of both gas and particle were obtained at different time intervals. The results show the evolution of the muzzle blast flow with gas-particle mixtures and demonstrate the effects of key parameter on the flow field of the gas-particle flow. This paper is a significant investigation for understanding the muzzle blast flow with gas-particle mixtures, which can provide valuable reference for the research on the muzzle blast flow.

Keywords: Computational fluid dynamics, Muzzle blast flow, Two-phase flow, Gas-particle mixtures.

1. INTRODUCTION

The propellant gas discharges from a cannon muzzle when launching the projectile, which affect firing crew safety and projectile accuracy. The propellant gas develops and forms a complex blast flow field near the cannon muzzle, which have the characteristics of unsteady flow, strong shock discontinuity and severe chemical reactions. This problem is schematically shown in Fig. 1, where several wave phenomena are defined, such as blast wave, incident shock, reflected shock, and Mach disk. It is important to study the mechanism of muzzle blast flow to improve or increase the efficiency of weapon.

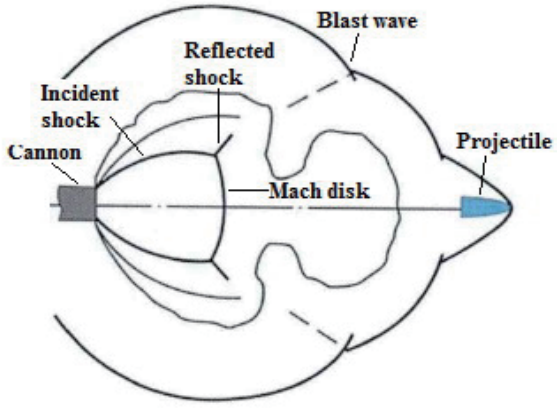


Fig. 1 Schematic of muzzle flow with moving projectile.

There are many investigations on the muzzle blast flow [1-13] in the past years, including theory, numerical simulation, and experiment. For instance, Wang *et al*. [5] simulated numerically the time-dependent behavior of the blast flow environment from an open cylindrical shock tube. The numerical results verified the adequacy of using an accurate inviscid approach to describe the features of the near-field vortex flow and time evolution of blast flow fields. Cler [8] adopted the fluent 6.1solvers and DG solver to simulate the muzzle flow without projectile. Shock waves dynamics process of the muzzle flow was numerically visualized in detail through special treatment on the moving cylinder projectile in the shock wave tube by Jiang ZL *et al*. [10]. Jiang XH *et al*. [12] simulated numerically the integrative process of a quiescent projectile accelerated by high-pressure gas to shoot out at a supersonic speed and beyond the range of a precursor flow field.

For numerical simulation studies of the muzzle blast flow previously, researchers did not consider the effect of solid particles in the propellant gas on the muzzle blast flow. In fact, the propellant gas pushed the projectile in the cannon is generated by the combustion of

* Corresponding author (njust203zcf@126.com)

DOI : 10.1017/jmech.2015.44
Copyright © 2015 The Society of Theoretical and Applied Mechanics, R.O.C.
https://doi.org/10.1017/jmech.2015.44 Published online by Cambridge University Press

solid gunpowder. However, part of the solid gunpowder did not completely burn, so the propellant gas contains great amount of solid particles. As is well-known, the flow of gases with solid particles are quite different from their pure gas counterparts due to momentum and energy exchange between the two phase. The solid particles cannot follow rapid changes in the gas velocity and temperature [14]. For the muzzle blast flow in this paper, the interaction between the solid particles and gas affects the muzzle blast flow and the launching process of projectile. So we cannot neglect the influence of the solid particles in the flow filed, and it is necessary to research the muzzle blast flow with gas-particle mixtures. In addition, it is difficult to study the launching process and obtain data by experimental methods since there is a very short time when the projectile moves from the muzzle to the surroundings. On the other hand, due to the rising cost of experimental measurements together with limited experimental facilities and testing technology, it is a great significance to establish a reasonable calculation method for the muzzle blast flow with gas-particle mixtures.

There are two numerical approaches to analyze the two-phase flow, the Eulerican-Lagrangian (E-L) approach and the Eulerian-Eulerian (E-E) approach. The difference between the two approaches is the way how the solid particles cloud is treated. In the E-L approach the particles are modeled directly as points moving due to the drag force acting on them from the surrounding gas and colliding. In the E-E approach the solid particles cloud is simulated as a second fluid with parameters like bulk density, velocity and temperature. Using E-E approach to study the blast flow with gas-particle mixtures is quite popular and effective. For instance, Wu [15] revealed the changes of diffraction pattern due to particle presence using E-E approach, and discussed the effects of particle properties on post-shock flow field. Fedorov [16] simulated numerically the shock and detonation wave diffraction at a sudden expansion in gas-particle mixtures using E-E approach. The influence of the size and mass loading of particles on the flow and shock wave structure behind the backward-facing step was studied and analyzed.

According the characteristics of solid gunpowder, the propellant gas are treated as a two-phase dispersed mixture of gas and contiguous particles, and the E-E approach are selected to study the muzzle blast flow with gas-particle mixtures. The propellant flow contains great amount of solid particles with different diameters, which are poly-dispersed particles. There are some references [17-19] for a poly-disperse Eulerian-Eulerican approach. The references consider poly-disperse modeling and the particle size distributions. As an early study of two-phase flow about the gun muzzle, we only consider the effect of a single size of the particles on the muzzle flow assuming the particles are mono-dispersed. The present study aim at research the evolution of the muzzle blast flow with gas-particle mixtures and demonstrate the effects of key parameter on the flow field of the gas-particle flow, so the calculation neglect the movement of projectile. The paper is organized as follows. In the next section, a reasonable calculation method for solving the muzzle blast flow with gas-particle mixtures are presented. After that, the computational model and boundary conditions are described. In Section 4, the muzzle blast flow with pure gas and gas-particle mixtures are computed. The particle diameter and the mass fraction of particle are tested to show their effects on the development process of the muzzle blast flow with gas-particle mixtures. The distribution of the main flow parameters of gas and particle are obtained at different time intervals. The results show the evolution of the muzzle blast flow with gas-particle mixtures and demonstrate the effects of key parameter on the flow field of the gas-particle flow. Finally conclusions from this study are summarized in Section 5.

2. MATHEMATICAL METHOD

2.1 Governing Equations

The following assumptions are universally adopted in the studies of gas-particle flow. We follow them as well:

- The gas obeys the perfect equation of state;
- The gas contains a variety of gaseous species (Air: $N_2 + O_2$; The propellant gas: $CO + CO_2 + H_2 + H_2O + H + O + OH + N_2$);
- The particles' volume is negligible;
- Particles do not collide with each other so that they do not contribute to pressure;
- Particles are spherical and of the same diameter; the density of particles' material is constant;
- Particles are inert;
- The gravity on particles are neglected;
- Momentum and heat transfer are taken into account only between the gas and particles.

Under these conditions, the basic equations governing gas-particle motion can be expressed as the conservation laws of mass, momentum and energy for each phase:

$$\begin{cases} \dfrac{\partial \boldsymbol{U}_g}{\partial t} + \dfrac{\partial \boldsymbol{F}_g}{\partial x} + \dfrac{\partial \boldsymbol{G}_g}{\partial y} + \boldsymbol{H}_g = \boldsymbol{S}_g + \boldsymbol{I}_g & \text{for gas phase} \\ \dfrac{\partial \boldsymbol{U}_p}{\partial t} + \dfrac{\partial \boldsymbol{F}_p}{\partial x} + \dfrac{\partial \boldsymbol{G}_p}{\partial y} + \boldsymbol{H}_p = \boldsymbol{I}_p & \text{for particle phase} \end{cases} \tag{1}$$

where $\boldsymbol{U}_g$, $\boldsymbol{U}_p$ are the vector of the conservative variables of gas phase and particle phase, $\boldsymbol{F}_g$, $\boldsymbol{G}_g$ are the vector of the convective fluxes of gas phase, $\boldsymbol{F}_p$, $\boldsymbol{G}_p$ are the vector of the convective fluxes of particle phase, $\boldsymbol{S}_g$ is the vector of source term caused by chemical reactions, $\boldsymbol{H}_g$ is the vector of source term of gas phase caused by axial symmetry, $\boldsymbol{H}_p$ is the vector of source term of particle phase caused by axial symmetry, $\boldsymbol{I}_g$, $\boldsymbol{I}_p$ are the vector of interaction source term between gas phase and particle phase. Here, the main vector are given by

https://doi.org/10.1017/jmech.2015.44 Published online by Cambridge University Press

$$\begin{cases} \boldsymbol{U}_g = \begin{bmatrix} \rho_1 \\ \vdots \\ \rho_{ns-1} \\ \rho \\ \rho u \\ \rho v \\ \rho E \end{bmatrix} \boldsymbol{F}_g = \begin{bmatrix} \rho_1 u \\ \vdots \\ \rho_{ns-1} u \\ \rho u \\ \rho u^2 + p \\ \rho uv \\ (\rho E + p)u \end{bmatrix} \boldsymbol{G}_g = \begin{bmatrix} \rho_1 v \\ \vdots \\ \rho_{ns-1} v \\ \rho v \\ \rho uv \\ \rho v^2 + p \\ (\rho E + p)v \end{bmatrix} \\ \boldsymbol{H}_g = \frac{1}{y} \begin{bmatrix} \rho_1 v \\ \vdots \\ \rho_{ns-1} v \\ \rho v \\ \rho uv \\ \rho v^2 \\ (\rho E + p)v \end{bmatrix} \boldsymbol{S}_g = \begin{bmatrix} \omega_1 \\ \vdots \\ \omega_{ns-1} \\ 0 \\ 0 \\ 0 \\ 0 \end{bmatrix} \boldsymbol{I}_g = \begin{bmatrix} 0 \\ \vdots \\ 0 \\ 0 \\ -f_x \\ -f_y \\ -f_x u_\mathrm{p} - f_y v_\mathrm{p} - Q \end{bmatrix} \end{cases} \tag{2}$$

$$\begin{cases} \boldsymbol{U}_\mathrm{p} = \begin{bmatrix} \rho_\mathrm{p} \\ \rho_p u_\mathrm{p} \\ \rho_p v_\mathrm{p} \\ \rho_\mathrm{p} E_\mathrm{p} \end{bmatrix} \boldsymbol{F}_\mathrm{p} = \begin{bmatrix} \rho_p u_\mathrm{p} \\ \rho_p u_\mathrm{p}^2 \\ \rho_p u_\mathrm{p} v_\mathrm{p} \\ \rho_\mathrm{p} E_\mathrm{p} u_\mathrm{p} \end{bmatrix} \boldsymbol{G}_\mathrm{p} = \begin{bmatrix} \rho_p v_\mathrm{p} \\ \rho_p u_\mathrm{p} v_\mathrm{p} \\ \rho_p v_\mathrm{p}^2 \\ \rho_\mathrm{p} E_\mathrm{p} v_\mathrm{p} \end{bmatrix} \\ \boldsymbol{H}_\mathrm{p} = \frac{1}{y} \begin{bmatrix} \rho_p v_\mathrm{p} \\ \rho_p u_\mathrm{p} v_\mathrm{p} \\ \rho_p v_\mathrm{p}^2 \\ \rho_\mathrm{p} E_\mathrm{p} v_\mathrm{p} \end{bmatrix} \boldsymbol{I}_p = \begin{bmatrix} 0 \\ f_x \\ f_y \\ f_x u_\mathrm{p} + f_y v_\mathrm{p} + Q \end{bmatrix} \end{cases} \tag{3}$$

In Eqs. (2) and (3), ρ is the density of the gas phase, p is the pressure of the gas phase, u, v are the components of the gas phase velocity, ρ_i is the density of species i in the gas phase. The subscripts i = 1, ..., ns-1,where ns is the total number of gas species. ω_i given by the chemical reaction kinetic model is the mass production rate of species i. ρ_p is the density of the particle phase, u_p, v_p are the components of the particle phase velocity, E_g and E_p are the total energy per unit mass of gas phase and particle phase, respectively. They are expressed as:

$$\begin{cases} E_g = \rho h - p + \frac{1}{2}\rho(u^2 + v^2) \\ E_p = c_v T_p + \frac{1}{2}\rho_p (u_p^2 + v_p^2) \end{cases} \tag{4}$$

where h is the special enthalpy of the gas phase, c_v is specific heat of the particle material, T_p is the temperature of particle phase.

The equation of state for a perfect gas with gas mixture constant R is expressed as:

$$p = \rho RT \tag{5}$$

where T is the temperature of the gas phase.

The components of the particle phase forces f_x, f_y and the heat transfer rate Q are expressed via the drag coefficient C_d and the Nusselt number Nu as:

$$\begin{cases} f_x = \frac{1}{8}\pi d_p^2 \rho (u - u_d)\sqrt{(u-u_d)^2 + (v-v_d)^2}\, C_d \\ f_y = \frac{1}{8}\pi d_p^2 \rho (v - v_d)\sqrt{(u-u_d)^2 + (v-v_d)^2}\, C_d \end{cases} \tag{6}$$

$$Q = \frac{\pi d_p C_p Nu}{\mathrm{Pr}}(T - T_p) \tag{7}$$

where d_p represents the particle diameter, and C_p represents the specific heat of the gas mixtures. The Prandtl number of the gas is assumed to be constant, Pr = 0.75.

In Eqs. (6) and (7), the drag coefficient C_d and the Nusselt number Nu depend on the particle Reynolds number Re. They are expressed as [14]:

$$C_d = 0.48 + 28Re^{-0.85} \tag{8}$$

$$Nu = 2.0 + 0.6Pr^{\frac{1}{3}}Re^{0.5} \tag{9}$$

where the particle Reynolds number is defined as:

$$Re = \frac{\rho d_p \sqrt{(u-u_p)^2 + (v-v_p)^2}}{\mu} \tag{10}$$

In this study, it is assumed that the viscosity coefficient and heat transfer rate depend only on temperature. The following formula is used for the viscosity coefficient [14]:

$$\mu = 1.71 \cdot 10^{-5} \left(\frac{T}{273.0}\right)^{0.77} \tag{11}$$

2.2 Numerical Methods

The terms representing the interaction between the gas and particle, and causing by chemical reactions among gas species are the source terms in the governing equations. These terms are handled using the operator splitting technique [20,21] for dealing with the stiff problem. The governing equations are decomposed as follows:

$$\begin{cases} \frac{\partial \boldsymbol{U}_g}{\partial t} + \frac{\partial \boldsymbol{F}_g}{\partial x} + \frac{\partial \boldsymbol{G}_g}{\partial y} + \boldsymbol{H}_g = 0 \\ \frac{\partial \boldsymbol{U}_p}{\partial t} + \frac{\partial \boldsymbol{F}_p}{\partial x} + \frac{\partial \boldsymbol{G}_p}{\partial y} + \boldsymbol{H}_p = 0 \end{cases} \tag{12}$$

$$\begin{cases} \frac{\partial \boldsymbol{U}_g}{\partial t} = \boldsymbol{S}_g + \boldsymbol{I}_g \\ \frac{\partial \boldsymbol{U}_p}{\partial t} = \boldsymbol{I}_p \end{cases} \tag{13}$$

The solution is then obtained in two steps. The Eq. (12) are solved, neglecting the interaction between the phases and chemical reaction between the gases. Then the solutions are modified by Eq. (13), taking into consideration the effect of the interaction and chemical reaction. The Eq. (13) are solved with the fourth order Runge-Kutta method. In order to avoid numerical

https://doi.org/10.1017/jmech.2015.44 Published online by Cambridge University Press

instabilities, the time step is determined based on CFL condition to satisfy the stability requirement.

Because the flow for the gas and particle phase possess different physical features and the solid particles have much larger inertia than the gas molecule. Hence, for the solution of Eq. (12) two numerical methods are applied respectively to the gas and particle equations.

For the gas phase, due to the presence of shock discontinuity, we adopt the AUSMPW+ scheme [22,23] to solve the gas equations. In order to improve the accuracy of spatial discretization, we should reconstruct the primitive variables before computing the convection flux quantities of the governing equation using upwind scheme. For the methods for reconstructing the primitive variables, the NND scheme [24] is used.

For the particle phase, due to the continuous change of the flow parameters across the shock front, the second-order MacCormack scheme [25] is employed.

Predictor step: In the predictor step, a "provisional" value at time level $n + 1$ is estimated as follows:

$$\tilde{U}_p^{n+1}\Big|_i = \boldsymbol{U}_p^n - \frac{\Delta t}{\Delta x}\left(\boldsymbol{F}_p^n\Big|_{i+1} - \boldsymbol{F}_p^n\Big|_i\right) - \frac{\Delta t}{\Delta y}\left(\boldsymbol{G}_p^n\Big|_{j+1} - \boldsymbol{G}_p^n\Big|_j\right) - \Delta t\, \boldsymbol{H}_p^n\Big|_i \tag{14}$$

Corrector step: In the corrector step, the predicted value is corrected according to the following equation:

$$\boldsymbol{U}_p^{n+1}\Big|_i = \frac{1}{2}\left(\boldsymbol{U}_p^n\Big|_i + \tilde{\boldsymbol{U}}_p^{n+1}\Big|_i - \frac{\Delta t}{\Delta x}\left(\tilde{\boldsymbol{F}}_p^n\Big|_i - \tilde{\boldsymbol{F}}_p^n\Big|_{i-1}\right) - \frac{\Delta t}{\Delta y}\left(\tilde{\boldsymbol{G}}_p^n\Big|_j - \tilde{\boldsymbol{G}}_p^n\Big|_{j-1}\right) - \Delta t\, \tilde{\boldsymbol{H}}_p^n\Big|_i\right) \tag{15}$$

2.3 Chemical Reaction Kinetic Model

One of the keys to determine the success of chemical non-equilibrium flow simulation is the chemical reaction kinetic model. In the current work, the chemical reaction kinetic model of Carbon Monoxide Oxidation involves 8 species (CO, H_2, O_2, CO_2, H_2O, H, OH, O), 1 inert specie (N_2) and 12 elementally reactions steps [26].

3. COMPUTATIONAL MODEL AND BOUNDARY CONDITION

The present study aim at research the evolution of the muzzle blast flow with gas-particle mixtures and demonstrate the effects of key parameter on the flow field of the gas-particle flow, so the movement of projectile is neglected in the calculation. The overall computational domain of the muzzle blast flow is shown in Fig. 2. The diameter of the cannon tube is 130mm, the length of cannon tube is 6m, the right boundary of the computational domain is 5m downstream from the cannon, and the distance between top boundary of the computational domain and symmetrical axis is 3m. According to the symmetry, only half of the physical model is calculated.

Figure 2 also shows the initial state of the calculation, and this time is defined as $t = 0.0$s. The blue area and red area represent the ambient air and the propellant gas with particles, respectively. According to the law of interior ballistics of a cannon, the velocity of the propellant gas in the cannon tube linearly varies with distance. The velocity of the propellant gas in the bottom of cannon is zero, while the velocity of propellant gas in the muzzle of the cannon is V_0 = 800m/s, which is equal to the initial velocity (launching velocity) of projectile when the projectile leaves the muzzle of the cannon. The temperature of the propellant gas is 2000K, and the pressure is P_0 = 40MPa. The temperature and velocity of the particles in the propellant gas are the same as the propellant gas. The particle density is dependent on the density of propellant gas and the mass fraction of the particles in the propellant gas. The composition of the propellant gas are shown in Table 1.

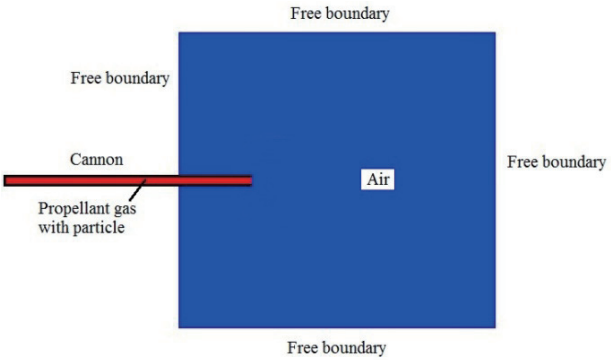


Fig. 2 Schematic of overall computational domain.

There are three boundary conditions, the solid, free boundary and axial symmetric boundary. The solid boundary include the inner and outer surfaces of the cannon tube. Both of these are assumed as slip boundaries, *i.e.*, and the normal velocity component of the solid boundary is zero. Since the free boundary is only affected by the interior, its interface flux is always equal to the flux of the cell-centered values. The axial symmetric boundary is the same as a solid boundary because the solid boundary is a slip boundary.

At the initial time $t = 0.0$s, the ambient air conditions near the cannon are at P_a = 1atm and T_a = 293K. The composition and mass fraction of Air is N_2-0.77, O_2-0.23, respectively. The particle density in ambient air is zero.

Table 1 The composition and mass fraction of propellant gas.

Composition	CO	H_2	CO_2	H_2O	N_2
Mass fraction	0.5138	0.0157	0.2153	0.1293	0.1259

4. NUMERICAL RESULTS AND DISCUSSION

4.1 The Development Process of the Muzzle Blast Flow with Pure Gas Phase

For the comparison with the gas-particle flow, the pure gas flow is simulated at first. We select the re-

https://doi.org/10.1017/jmech.2015.44 Published online by Cambridge University Press

sults of the pure gas flow to indicate the development process of the muzzle blast flow.

After the projectile leaves the muzzle of cannon, the propellant gas with high temperature and high pressure in the cannon tube is suddenly released and rushes out. Meanwhile, the propellant gas flow, the initial environmental ambient air flow mutually couple and interact. The numerical results are presented in a time sequence in Fig. 3, which plot the temperature contours and Mach number contours of pure gas phase flow. Figure 3(a) shows the flow field at t = 0.5ms. The propellant gas quickly propagates into the external ambient air, and starts to expand and accelerate, leading to a decrease of temperature, and an increase of Mach number. It is also observed that, there is a high-temperature zone near the contact surface (it is located between the propellant gas and the external air), resulting from the secondary combustion of the CO/H_2 in the propellant gas with the O_2 in the external air. According to Fig. 3(b) at t = 1.5ms, a complete Mach disk is formed, and a typical jet flow structure is observed, including blast wave, incident shock, shear layer, primary vortex ring, and triple point. It is also observed that the high-temperature zone near the contact surface disappears, shown that the degree of the secondary combustion near the contact surface weakens gradually. The reason for the secondary combustion weakening gradually is that both the concentration of combustible gas (including the CO and H_2) and pressure near the contact surface gradually decrease with the propagation of the propellant gas. It can be observed that Mach disk begins to fully develop at t = 2.5ms in Fig. 3(c). This phenomenon means that the triple point and incident shock gradually converge toward the central axis, the diameter of Mach disk begins to decrease, and the temperature of gas behind Mach disk gradually increases. For example, the temperature of the gas behind Mach disk at t = 1.5ms is approximately 1600K, while the counterpart at t = 2.5ms is approximately 1800K. These phenomena are caused by the developing Mach disk.

4.2 The Effect of Particle Diameter on the Muzzle Blast Flow with Gas-Particle Mixtures

The comparison of the main flow parameter in both pure gas flow and gas-particle flow with different particle diameter are shown in Fig. 4 (Gas temperature), Fig. 5 (Mach number) and Fig. 6 (Mass fraction of H_2O). The comparison of the main flow parameter of gas and particle in the gas-particle flow with different particle diameter are shown in Fig. 7 (Axial velocity) and Fig. 8 (Temperature). Temperature and axial velocity distribution for different particle diameter along the center axis near the muzzle are shown in Figs. 9 and 10, respectively.

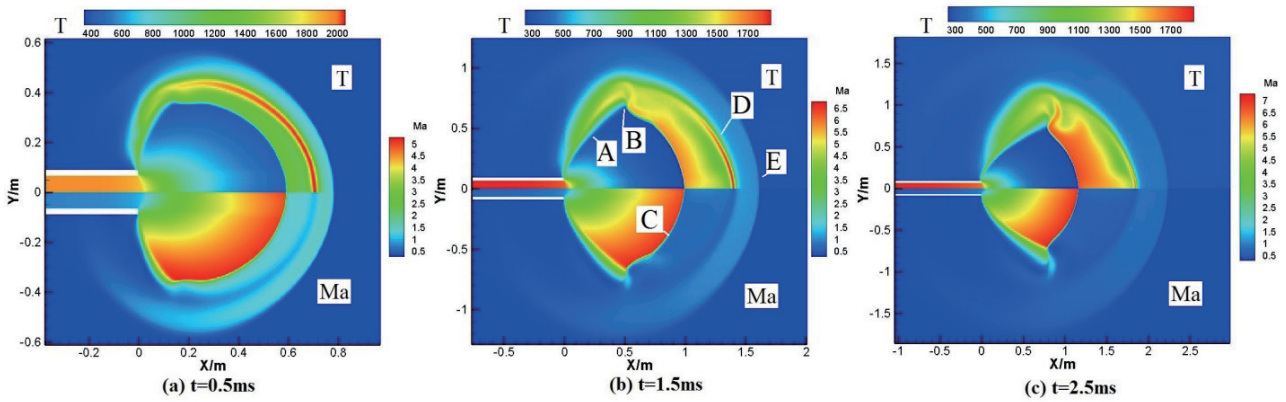


Fig. 3 A time sequence of temperature contours (Upper), Mach number contours (Lower) in pure gas phase flow: A-Incident shock; B-Triple point; C-Mach disk; D-Contact surface between propellant gas and air; E-Blast wave.

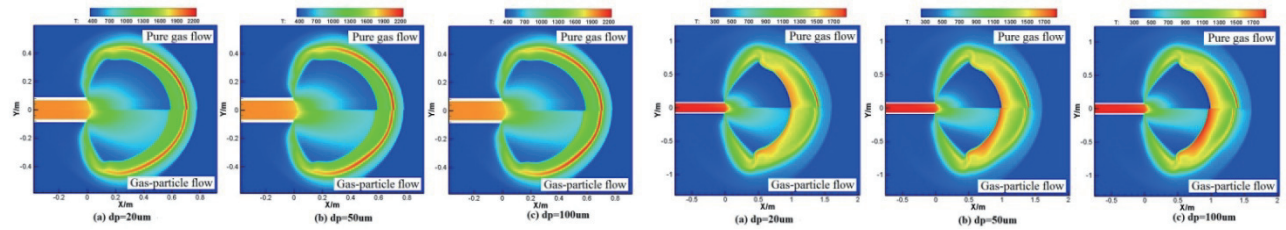


Fig. 4 The comparison of gas temperature in both pure gas flow and gas-particle flow with different particle diameter (Left: t = 0.5ms; Right: t = 1.5ms).

https://doi.org/10.1017/jmech.2015.44 Published online by Cambridge University Press

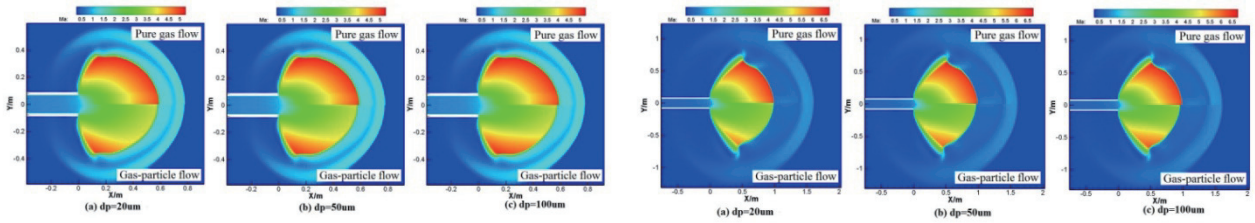


Fig. 5 The comparison of Mach number in both pure gas flow and gas-particle flow with different particle diameter (Left: t = 0.5ms; Right: t = 1.5ms).

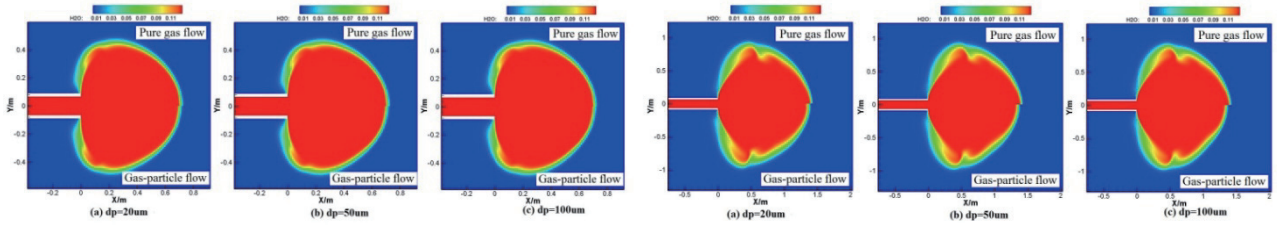


Fig. 6 The comparison of H_2O mass fraction in both pure gas flow and gas-particle flow with different particle diameter (Left: t = 0.5ms; Right: t = 1.5ms).

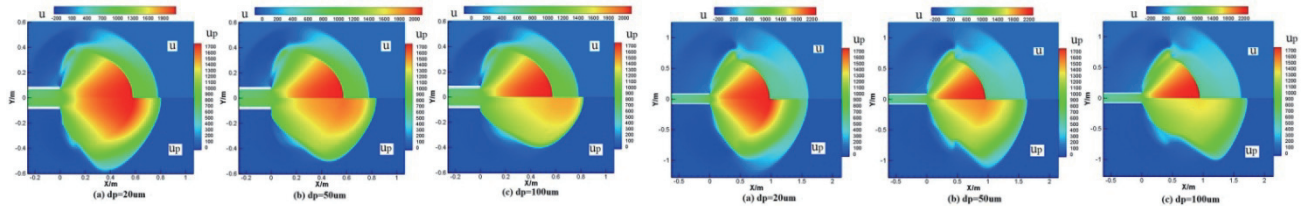


Fig. 7 The comparison of axial velocity of gas(u) and particle(u_p) in gas-particle flow with different particle diameter (Left: t = 0.5ms; Right: t = 1.5ms).

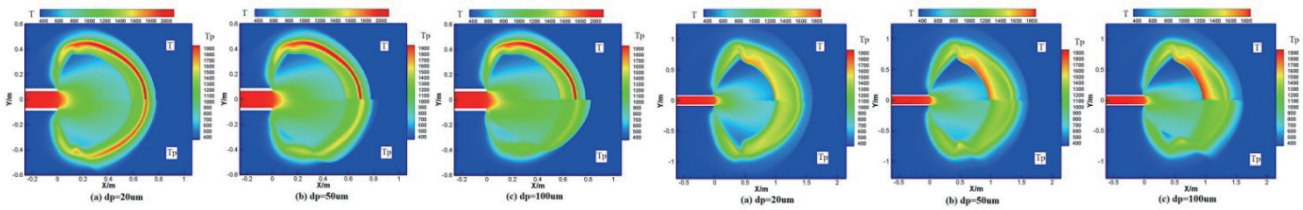


Fig. 8 The comparison of temperature of gas(T) and particle(T_p) in gas-particle flow with different particle diameter (Left: t = 0.5ms; Right: t = 1.5ms).

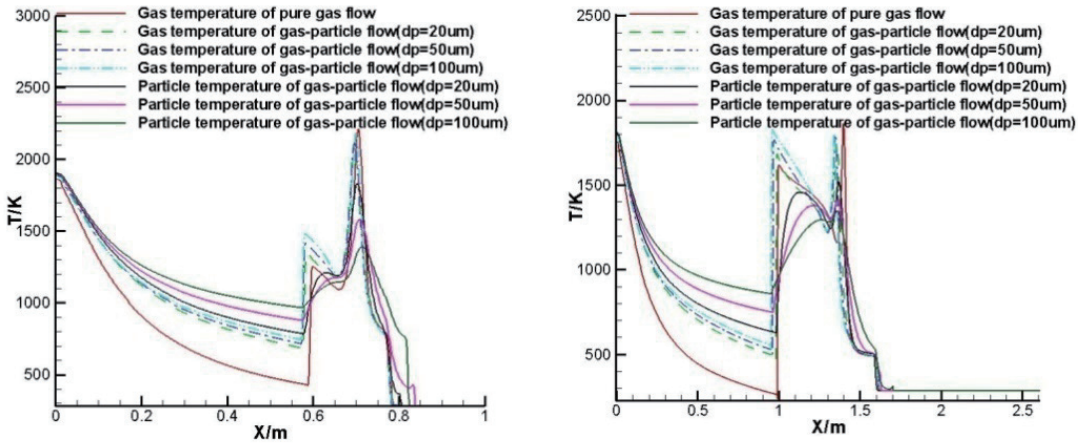


Fig. 9 Temperature distribution with different particle diameter along the center axis near the muzzle (Left: t = 0.5ms; Right: t = 1.5ms).

https://doi.org/10.1017/jmech.2015.44 Published online by Cambridge University Press

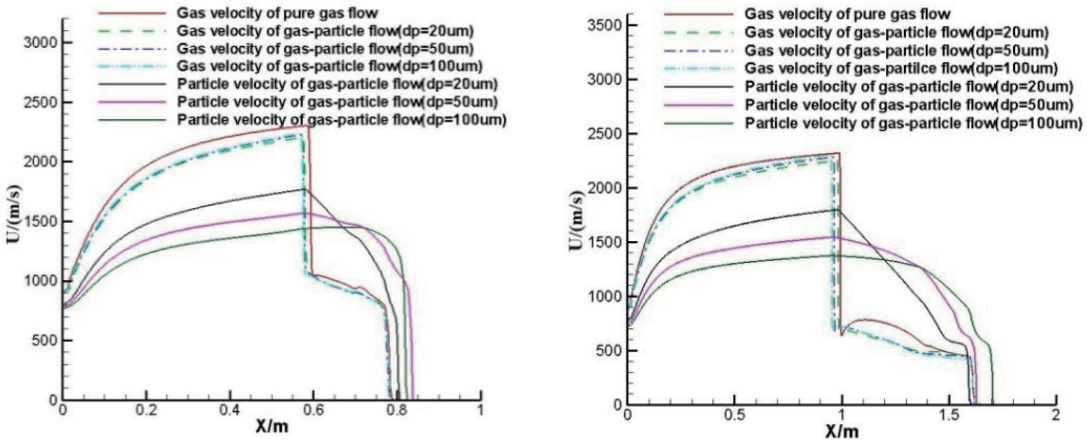


Fig. 10 Axial velocity distribution with different particle diameter along the center axis near the muzzle (Left: t = 0.5ms; Right: t = 1.5ms)

According to the results in Figs. 4 to 6, the development trend of the muzzle blast flow with gas-particle mixtures is nearly identical with that in the pure gas flow, and only the distribution of main flow parameters are different.

In front of Mach disk (The left of Mach disk), the high-temperature propellant gas discharges from the cannon tube and expands with a decrease of temperature. However, the particle phase has no such expansion and decreased temperature characteristic which is the same as the gas phase, resulting in a temperature difference between gas phase and particle phase. Thus, the heat transfer between the gas phase and particle phase cause the particle to gradually cool, while the temperature of the particle phase is always much higher than that of gas phase due to thermal hysteretic nature of particle. At this time, the gas phase is heated by the particle phase and causes the gas temperature in gas-particle flow to be higher than the one in pure gas flow. However, the larger the particle diameter, the greater the thermal hysteretic nature of particle. For large particle diameter, it means the particle phase is not easily cooled by the gas phase. In other words, it can been seen from the temperature distribution in Fig.9, the temperature of both particle phase and gas phase increase with the increase of particle diameter at an arbitrary position along center axis.

Behind Mach disk (The right of Mach disk), although the gas temperature in both pure gas flow and gas-particle flow rise sharply, the gas peak temperature near Mach disk in gas-particle flow is higher than the one in pure gas flow. The larger the particle diameter, the higher the gas peak temperature near Mach disk in gas-particle flow. However, the gas phase begins to heat the particle phase conversely since the gas temperature is greater than the particle temperature in gas-particle flow. It can be observed that the particle temperature behind Mach disk in gas-particle flow with particle diameter of 20μm is highest. This is because with the decrease of the particle diameter, the thermal hysteretic nature of particle become weak, and the gas phase has much stronger capacity to heat particle phase. In addition, the gas temperature near contact surface increases obviously due to the secondary combustion, and the high-temperature gas begins to heat the particle phase. However, the gas temperature near contact surface in gas-particle flow is always lower the counterpart in pure gas flow and decreases gradually with the increase of particle diameter.

In front of Mach disk, the particle phase moves with the movement of the gas phase due to the drag force. While the change of the particle velocity has a certain relaxation time because of its own inertia, leading the particle velocity significantly to lag behind the gas velocity. When the particle diameter is small, the inertia of particle is also small, and the momentum transport between the gas phase and the particle phase is much stronger, meaning the velocity lag between the gas phase and the particle phase is relatively small. In a short, at an arbitrary position along center axis, the velocity of the particle increases with the decrease of particle diameter, which is shown in Fig. 10. As is shown in Fig. 5, in the area near the center axis the Mach number in gas-particle flow is far lower than that in pure gas flow. The reason for this phenomenon is that the distribution of gas temperature near the center axis in gas-particle flow is higher than the one in pure gas flow, while the distribution of velocity is lower than the one in pure gas flow. In addition, as can be seen from the results in Fig. 10, the axial velocity of gas in gas-particle flow with different particle diameter are nearly identical and always lower than the axial velocity of gas in pure flow. The distance between Mach disk and the cannon muzzle in gas -particle flow is much smaller than the distance in pure gas flow.

Behind Mach disk, the gas velocity and Mach number sharply decrease, and the gas temperature sharply rises. However, the particle velocity does not have drastically change due to its own inertia and incompressible nature. The larger the particle diameter, the larger the inertia of particle. For the gas-particle flow with the large diameter particle of 100μm, the particle phase continues to accelerate in some distance and then gradually decelerates. In a contrary, for the gas-particle flow with the small diameter particle of 20μm, the particle phase immediately decelerates through Mach disk due to the effect of the change of the gas velocity.

https://doi.org/10.1017/jmech.2015.44 Published online by Cambridge University Press

As can be seen from the axial velocity contours and axial velocity distribution along center axis in Figs. 7 and 10, the gas velocity gradually decreases to zero through Mach disk at t = 0.5ms, and the location where the gas velocity is zero is the gas blast wave. However, as be discussed in above paragraph, the particle velocity is larger than the gas velocity along the center axis between Mach disk and the gas blast wave, resulting the particle blast wave is further away from the cannon compared with the gas blast wave. At t = 1.5ms, the location of both the gas blast wave and the particle blast wave in the gas-particle flow with the particle diameter of 20μm are nearly identical. With the increase of the particle diameter, the location of the particle blast wave is significantly difference in the location of the gas blast wave. As can be seen from the axial velocity distribution along the center axis in Fig. 10, the location of the gas blast wave in pure gas flow and gas-particle flow with different particle diameter are nearly identical, indicating the particle phase only affect the distribution of the flow parameter between the muzzle and the gas blast wave, while it cannot affect the propagation speed of the gas blast wave.

In addition, as can be seen from the contours of the axial velocity of particle and the temperature of particle in Figs.7 and 8, with the increase of particle diameter, the inertia of particle will increase and then particle phase is more difficult to propagate along the radial direction after they rush out of the muzzle of cannon. So the shape of the particle blast wave in gas-particle flow with the particle diameter of 100μm is flat and the radial diameter of the particle blast wave is smaller than the one in gas-particle flow with the particle diameter of 20μm. Consequently, with large diameter of particle, the overall shape of particle phase flow filed is obviously different in the overall shape of gas phase flow field.

Since the composition of the propellant gas is different with the external air, so the mass fraction of H_2O in the propellant gas is chosen as a validition that reflects the propellant gas flow range. Figure 6 show the mass fraction countours of H_2O at different times. At t = 0.5ms, the location of the contact surface in both gas-particle flow and pure gas flow is a little different. While the contact surface in gas-particle flow always lags behind the one in pure gas flow at t = 1.5ms.

4.3. The Effect of the Mass Fraction of Particle on the Muzzle Blast Flow with Gas-Particle Mixtures

The comparison of the main flow parameter in both pure gas flow and gas-particle flow with different mass fraction of particle are shown in Fig. 11 (Gas temperature), Fig. 12 (Mach number) and Fig. 13 (Mass fraction of H_2O). The comparison of the main flow parameter of gas and particle in the gas-particle flow with different mass fraction of particle are shown in Fig. 14 (Axial velocity) and Fig. 15 (Temperature). Temperature and axial velocity distribution for different mass fraction of particle along the center axis near the muzzle are shown in Figs.16 and 17, respectively.

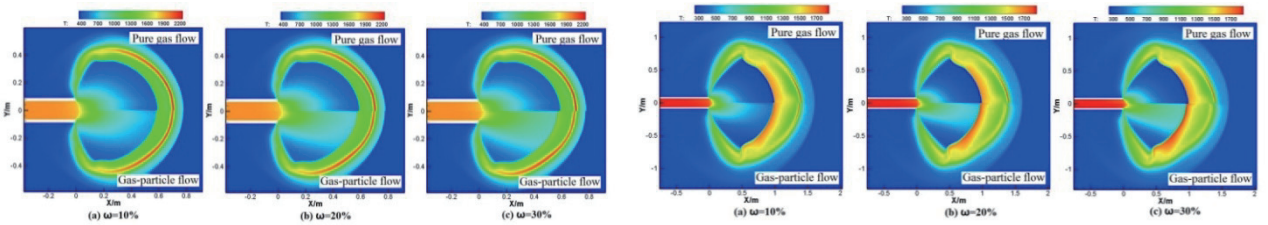


Fig. 11 The comparison of gas temperature in both pure gas flow and gas-particle flow with different mass fraction of particle (Left: t = 0.5ms; Right: t = 1.5ms).

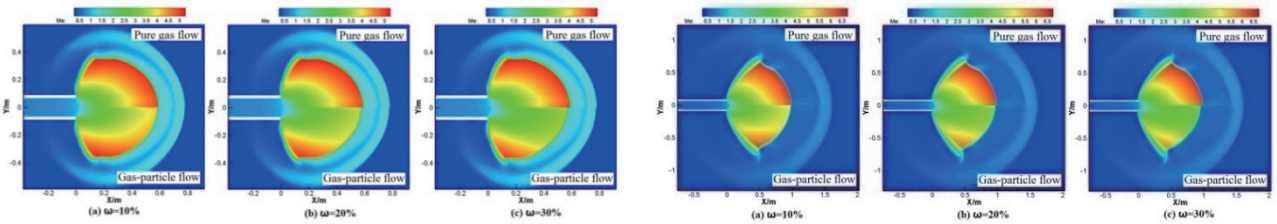


Fig. 12 The comparison of Mach number in both pure gas flow and gas-particle flow with different mass fraction of particle (Left: t = 0.5ms; Right: t = 1.5ms).

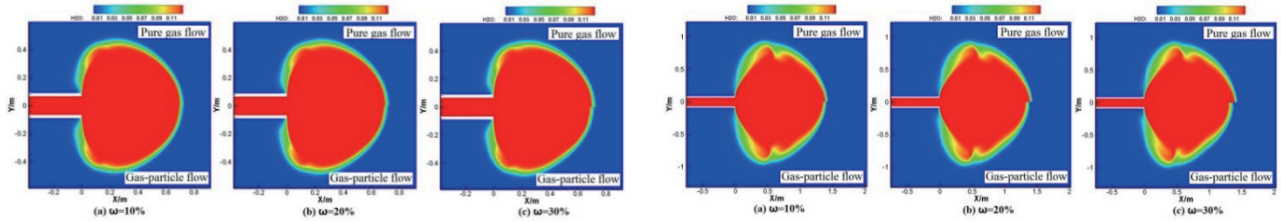


Fig. 13 The comparison of H_2O mass fraction in both pure gas flow and gas-particle flow with different mass fraction of particle (Left: t = 0.5ms; Right: t = 1.5ms).

https://doi.org/10.1017/jmech.2015.44 Published online by Cambridge University Press

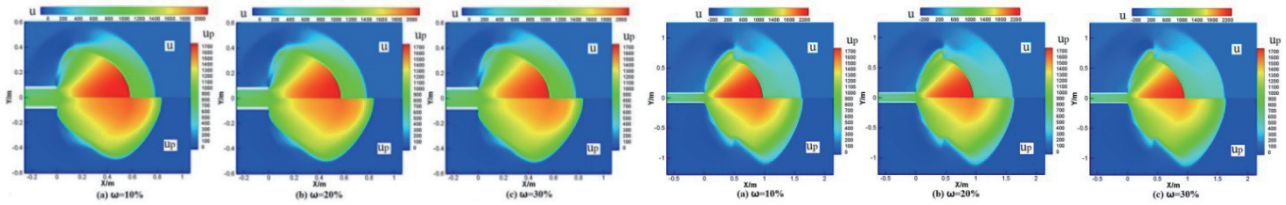


Fig. 14 The comparison of axial velocity of gas (u) and particle (u_p) in gas-particle flow with different particle diameter (Left: t = 0.5ms; Right: t = 1.5ms).

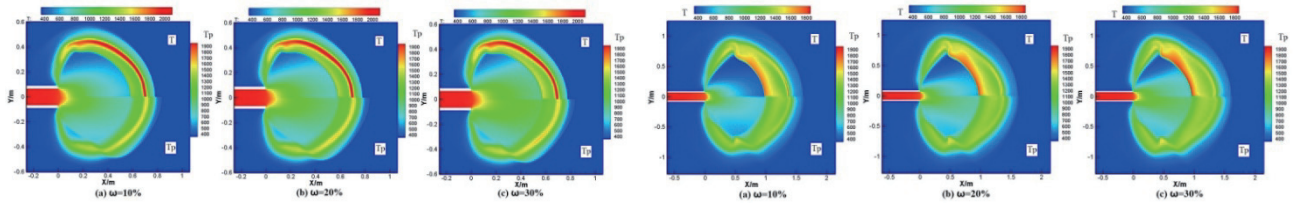


Fig. 15 The comparison of temperature of gas (T) and particle (T_p) in gas-particle flow with different particle diameter (Left: t = 0.5ms; Right: t = 1.5ms).

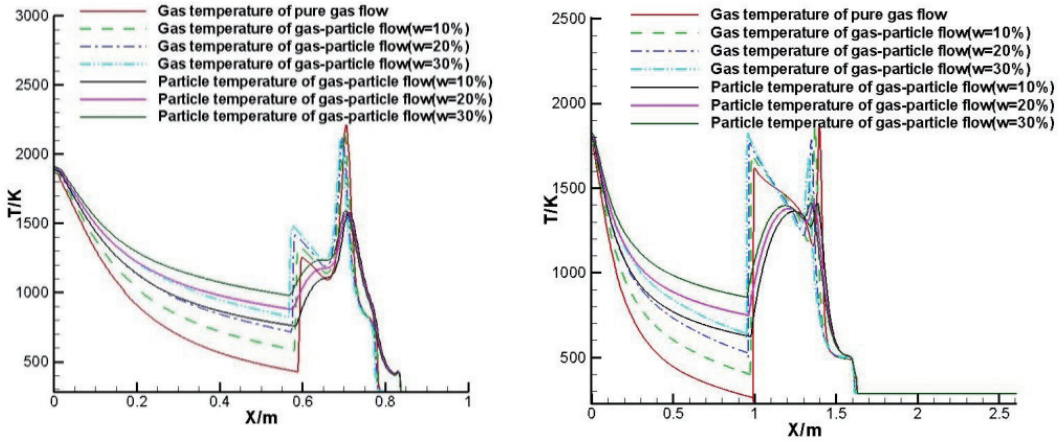


Fig. 16 Temperature distribution for different mass fraction of particle along the center axis near the muzzle (Left: t = 0.5ms; Right: t = 1.5ms).

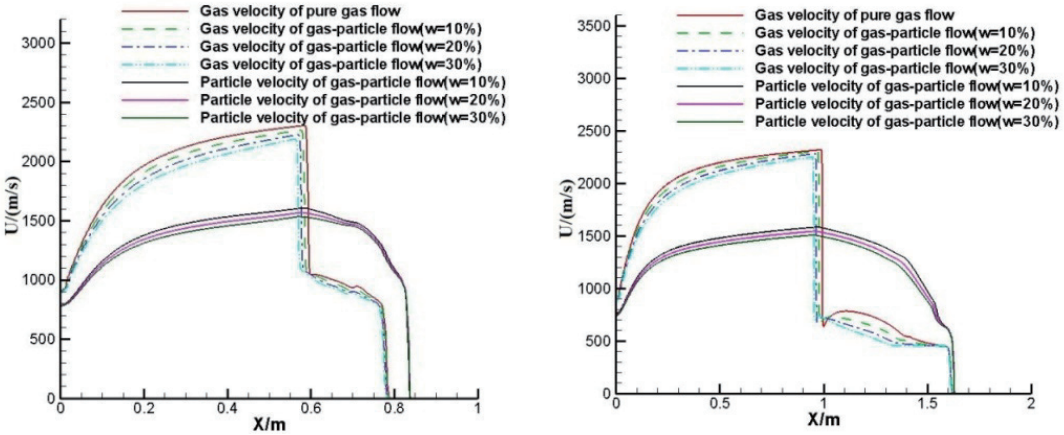


Fig. 17 Axial velocity distribution for different mass fraction of particle along the center axis near the muzzle (Left: t = 0.5ms; Right: t = 1.5ms).

It's well-known that, if the mass fraction of particle is much higher, the particle number per unit volume are greater. It means that the particle phase carry more energy itself and transport more energy to the cooling gas. Therefore, with the increase of mass fraction of particle, the decreased degree of both gas temperature and particle temperature are much slower. As can be seen from the temperature contours and temperature distribution along center axis in Figs. 11, 15 and 16, the temperature of both particle and gas increase with the increase of mass fraction of particle at an arbitrary position along center axis, and the temperature of particle is also always higher than the temperature of gas. The heat generated by the secondary combustion near contact surface is transported to the particle phase and the extent of heat transfer increases with the increase of the

https://doi.org/10.1017/jmech.2015.44 Published online by Cambridge University Press

mass fraction of particle. So the gas temperature near contact surface gradually decreases with the increase of mass fraction of particle as is shown in Figs.11 and 16.

As can be seen from the axial velocity contours and axial velocity distribution along center axis in Figs. 15 and 17, with the increase of mass fraction of particle, the acceleration degree of both gas phase and particle phase are much lower (The velocity of both particle and gas decrease gradually with the increase of mass fraction of particle at an arbitrary position along center axis). However, with the increase of mass fraction of particle, the gas phase is more difficult to accelerate the particle phase. Consequently, the gas phase suffer more severe drag force generated by particle phase with higher mass fraction of particle, resulting in both the gas velocity and particle velocity decrease gradually at an arbitrary position along center axis.

Although the particle velocity with different mass fraction of particle have some difference in front of Mach disk, they are basically same in some distance behind Mach disk, and the location of the particle blast wave are also nearly identical.

With different mass fraction of particle, the particle blast wave is always further away from the cannon muzzle than the gas blast wave at the time $t = 0.5$ms. While both the gas blast wave and particle blast wave are nearly identical at the time $t = 1.5$ms.

As can be seen from the axial velocity distribution along center axis in Fig. 17, the location of gas blast wave in both pure gas flow and gas-particle flow with different mass fraction of particle are nearly identical. This phenomenon indicates that the particle phase only affect the flow parameter distribution between the muzzle and the front of gas blast wave, while it cannot affect the propagation speed of the gas blast wave under the conditions of different particle diameter or different mass fraction of particle.

The location of the contact surface in gas-particle flow with the mass fraction of 10% is nearly identical with the location of the contact surface in pure gas flow at $t = 0.5$ms. With the increase of mass fraction of particle, the distance between the contact surface and the cannon muzzle in the gas-particle flow is much smaller than the distance in pure gas flow, meaning the movement of contact surface in gas-particle flow lags behind the counterpart in the pure gas flow. Although the contact surface in gas-particle flow with different mass fraction of particle always lags behind the contact surface in pure gas flow at $t = 1.5$ms, the distance between the contact surface and the cannon muzzle in gas-particle flow with different mass fraction of particle have no significant difference.

5. CONCLUSIONS

The issue on the muzzle blast flow with gas-particle mixture is numerically investigated using the E-E approach in this paper. The particle diameter and the mass fraction of particle are tested to show their effects on the development process of the muzzle blast flow with gas-particle mixtures. The conclusions are summarized as follows:

(1) The development trend of the muzzle blast flow with gas-particle mixtures is nearly identical with that in the pure gas flow, and only the distribution of main flow parameters are different. In front of Mach disk, the gas phase is heated by particle phase and it causes the gas temperature in gas-particle flow to be higher than the one in pure gas flow. However, the larger the particle diameter, the greater hysteretic nature of particle. For large particle diameter, it means the particle phase is not easily cooled by the gas phase. When the particle diameter is small, the inertia of particle phase is also small, and the momentum transport between the gas phase and the particle phase is much stronger, meaning the velocity lag between the gas phase and particle phase is relatively small.

(2) Behind Mach disk, although the gas temperature in both pure gas flow and gas-particle flow rise sharply, the gas peak temperature near Mach disk in gas particle flow is higher than the one in pure gas flow. The larger the particle diameter, the higher the gas peak temperature near Mach disk in gas-particle flow. The gas velocity and Mach number sharply decrease, and the gas temperature sharply rise. The particle velocity does not have drastically change due to its own inertia and incompressible nature. For the gas-particle flow with the large diameter particle of 100μm, the particle continues to accelerate due to the effect of the change of the gas phase velocity in some distance and then gradually decelerates. In a contrary, for the gas-particle flow with the small diameter particle of 20μm, the particle immediately decelerates through Mach disk.

(3) The location of the gas blast wave in both pure gas phase flow and gas-particle flow with different mass fraction of particle or different particle diameter are nearly identical. This phenomenon indicates that the particle only affect the distribution of the flow parameter between the muzzle and the gas blast wave, while it cannot affect the propagation speed of the gas blast wave under the conditions of different particle diameter or different mass fraction of particle. Under the conditions of different mass fraction of particle, the location of particle blast wave are nearly identical at the time $t = 0.5$ms or $t = 1.5$ms.

ACKNOWLEDGEMENTS

This work has been financially supported by the National Natural Science Foundation of China (Grant No.11402119) and the Funding of Jiangsu Innovation Program for Graduate Education (Grant No. CXLX13-202).

REFERENCES

1. Schmidt, E. M. and Shear, D., "Optical Measurements of Muzzle Blast," *AIAA Journal*, **13**, pp. 1086–1091 (1975).

https://doi.org/10.1017/jmech.2015.44 Published online by Cambridge University Press

2. Fansler, K. S. and Schmidt, E. M., "Trajectory Perturbations of Asymmetric Fin-Stabilized Projectiles Caused by Muzzle Blast," *Journal of Spacecraft and Rockets*, **15**, pp. 62–64 (1978).
3. Taylor, T. D. and Lint, T. C., "Numerical Model for Muzzle Blast Flow Fields," *AIAA Journal*, **19**, pp. 346–349 (1980).
4. Klingenberg, G., "Gun Muzzle Blast and Flash," *Propellants, Explosives, Pyrotechnics*, **14**, pp. 57–68 (1989).
5. Wang, J. C. T. and Widhopf, G. F., "Numerical Simulation of Blast Flow Fields Using a High Resolution TVD Finite Volume Scheme," *Computers & Fluids*, **18**, pp. 103–137 (1990).
6. Alziary, D. R. T., Cayac, R., Carette, E. and Balbo, P., "Theoretical and Comparison of Unsteady Flow Through a Muzzle Brake," *13th International Symposium on Ballistics*, Stockholm, Sweden (1992).
7. Jiang, Z. L., Takayama, K. and Skews, B. W., "Numerical Study on Blast Flowfields Induced by Supersonic Projectiles Discharged from Shock Tubes," *Physics of Fluids*, **10**, pp. 277–288 (1998).
8. Cler, D. L., Chevaugeon, N., Shephard, M. S. and Remacle, J. F., "CFD Application to Gun Muzzle Blast—A Validation Case Study," *AIAA Paper 2003–1142*, U.S.A. (2003).
9. Le, G. G., Ma, D. W. and Feng, Y., "Numerical Simulation of Muzzle Blast Flowfields of Large Caliber Guns," *Acta Armamentarii*, **25**, pp. 19–22 (2004).
10. Jiang, Z. L., Huang, Y. H. and Takayama, K., "Shocked Flow Induced by Supersonic Projectiles Moving in Tubes," *Computers & Fluids*, **33**, pp. 953–966 (2004).
11. Jiang, X. H., Fan, B. C. and Li, H. Z., "Numerical Investigation on the Muzzle Flow with Dynamic Mesh Based on ALE Equation," *Chinese Journal of Computational Mechanics*, **25**, pp. 563–567 (2008).
12. Jiang, X. H., Fan, B. C. and Li, H. Z., "Numerical Investigation on Dynamic Process of Muzzle Flow," *Applied Mathematics and Mechanics*, **29**, pp. 351–360 (2008).
13. Cayzac, R., Carette, E., De, Roquefort, T. A., Renard, F. X., Roux, D., Balbo, P. and Patry, J. N., "Computational Fluid Dynamics and Experimental Validation of the Direct Coupling Between Interior, Intermediate and Exterior Ballistics Using the Euler Equations," *Journal of Applied Mechanics-Transactions of the ASME*, **78**, pp. 1–20 (2011).
14. Saito, T., Marumoto, M. and Takayama, K., "Numerical Investigations of Shock Waves in Gas-Particle Mixtures," *Shock Wave*, **13**, pp. 299–322 (2003).
15. Wu, Q. S., Zhu, H. and Xu, Y. H., "Numerical Study of Shock Diffraction in Dusty Gases," *Applied Mathematics and Mechanics*, **16**, pp. 79–85 (1995).
16. Fedorov, A. V., Kratova, Y. V. and Khmel, T. A., "Shock and Detonation Wave Diffraction at a Sudden Expansion in Gas-Particle Mixtures," *Shock Waves*, **18**, pp. 281–290 (2008).
17. Doisneau, F., "Eulerian Modeling and Simulation of Polydisperse Moderately Dense Coalescing Spary Flows with Manometric-to-Inertial Droplets: Application to Solid Rocket Motors," Ph.D. Dissertation, CNRS et Ecole Central Paris, France (2013).
18. Doisneau, F., Laurent, F., Murrone, A., Dupays, J. and Massot, M., "Eulerian Multi-Fluid Models for the Simulation of Dynamics and Coalescence of Particles in Solid Propellant Combustion," *Journal of Computational Physics*, **234**, pp. 230–262 (2013).
19. Doisneau, F., Sibra, A., Dupays, J., Murrone, A., Laurent, F. and Massot, M., "Numerical Strategy for Unsteady Two-Way Coupling in Polydisperse Sprays: Application to Solid Rocket Motor Instabilities," *Journal of Propulsion and Power*, **35**, pp. 727–748 (2014).
20. Toro, E. F., *Riemann Solvers and Numerical Methods for Fluid Dynamics*, Springer, Heidelberg (1997).
21. Zhuo, C. F., Wu, X. S. and Feng, F., "Numerical Simulation of Supersonic Non-Equilibrium Flow Using Kinetic Scheme," *Journal of Ballistics*, **25**, pp. 88–94 (2013).
22. Kim, K. H., Kim, C. and Rho, O. H., "Accurate Computations of Hypersonic Flow Using AUSMPW+ Scheme and Shock-Aligned Grid Technique," *AIAA Paper 98–2442*, U.S.A. (1998).
23. Kim, K. H., Kim, C. and Rho, O. H., "Methods for the Accurate Computations of Hypersonic Flow: I. AUSMPW+ Scheme," *Journal of Computational Physics*, **174**, pp. 38–80 (2001).
24. Zhang, H. X., Chen, J. Q. and Gao, S. C., "Numerical Simulation of Supersonic Non-Equilibrium Flow for H_2/O_2 Combustion," *Journal of Astronautics*, **14**, pp. 14–23 (1994).
25. MacCormack, R. W., "The Effect of Viscosity in Hypervelocity Impact Cratering," *AIAA Paper 69–354*, U.S.A. (1969).
26. Gibeling, H. J. and Nietubicz, C. J., "Navier-Stokes Computations for Reacting, M864 Base Bleed Projectile," *AIAA Paper 93–0504*, U.S.A. (1993).

(Manuscript received October 15, 2014,
accepted for publication March 5, 2015.)

https://doi.org/10.1017/jmech.2015.44 Published online by Cambridge University Press